

Published in: J. Opt. A: Pure Appl. Opt. **5** (2003) 192–198

Online at: stacks.iop.org/JOptA/5/192

Dielectric multilayer waveguides for TE and TM mode matching

D M Shyroki and A V Lavrinenko

Physics Faculty, Belarusian State University, Fr. Scaryna Avenue 4, 220080 Minsk, Belarus

E-mail: shyroki@tut.by

Abstract. We analyse theoretically for the first time to our knowledge the perfect phase matching of guided TE and TM modes with a multilayer waveguide composed of linear isotropic dielectric materials. Alongside strict investigation into dispersion relations for multilayer systems, we give an explicit qualitative explanation for the phenomenon of mode matching on the basis of the standard one-dimensional homogenization technique, and discuss the minimum number of layers and the refractive index profile for the proposed device scheme. Direct applications of the scheme include polarization-insensitive, intermodal dispersion-free planar propagation, efficient fibre-to-planar waveguide coupling and, potentially, mode filtering.

As a self-sufficient result, we present compact analytical expressions for the mode dispersion in a finite, N -period, three-layer dielectric superlattice.

Keywords: Planar waveguides, dispersion relation, perfect phase matching

1. Introduction

Since the early experiments on mode conversion in film-waveguide magneto-optical systems [1, 2] and the subsequent theoretical works [3, 4, 5] it has become clear that an equality between propagation constants of the two guided modes—otherwise called mode matching or perfect phase matching—can be realized exclusively due to the tensorial character of dielectric permittivity of the waveguiding slab, i.e. due to its either natural or induced anisotropy. An obvious way to gain anisotropy is to produce a waveguide layer of monocrystalline material possessing intrinsic birefringence; another possibility is provided by use of gyrotropic waveguides (for example, YIG on GGG) subject to an external DC magnetic field. Historically, it was the latter way that experimentalists followed, probably because of its higher flexibility and technical reliability. A number of device schemes implementing that principle were rapidly proposed, from an optical switch [1] to a sensitive experimental method of determining the permittivity tensor elements [3]. The two unpleasant drawbacks were then the complexity of the schemes and the comparatively high absorption in gyrotropic films that hindered their utilization, e.g. for intermodal dispersion-free planar propagation.

On the other hand, in recent years a certain interest in traditional multilayer dielectric mirrors from the viewpoint of photonic bandgap localization has been observed, stimulated probably by the unexpected discovery of total omnidirectional reflection from an appropriately designed one-dimensional dielectric lattice, i.e. an actual photonic band gap exhibited in case of such a simple geometry [6, 7, 8, 9]. What looks now curious but is important for the purpose of the present treatment is that one can easily see the points of perfect phase matching of TE and TM modes on the standard band structure diagrams of dielectric multilayers [10, ch 4], yet unfortunately little or no attention has been paid in the literature to those mode matching phenomena—in spite of so many promising applications including polarization-insensitive, intermodal dispersion-free planar waveguiding, efficient fibre-to-planar waveguide coupling and, potentially, mode filtering, drastic improvement of mode conversion efficiency and diffraction efficiency in magneto-optical Bragg cells and others. To the best of our knowledge, the underlying idea that a multilayer waveguide can be regarded as a homogeneous, effectively anisotropic slab—and as if it were the case of a naturally birefringent or gyrotropic, magnetized waveguide, the perfect phase matching of TE and TM modes must occur—has been formulated just recently [11].

The aim of the current paper is to highlight and theoretically investigate the perfect phase matching of guided TE and TM modes with a multilayer device composed of linear, isotropic, non-magnetic and non-absorbing materials. The paper is organized as follows. Section 2 is devoted mainly to qualitative models and considerations: we begin with a transparent explanation for the mode matching phenomenon on the basis of conventional one-dimensional homogenization method and then discuss the general eigenproblem for TE and TM modes in order to derive some basic requirements for the scheme, such as the minimum number of layers and the proper refractive index profile.

Strict analytical expressions for the modal dispersion structure of periodic dielectric stacks with two-layer and three-layer unit cells follow those qualitative speculations and are given in section 3. Finally, we analyse in section 4 several examples of perfect phase matching with simple planar structures composed of silicon and silicon-nitride layers, fully compatible with modern integrated optics techniques.

2. What is mode matching by a multilayer dielectric waveguide?

A straightforward way to make the idea of perfect phase matching transparent is to consider a stack of isotropic dielectric layers as an effectively homogeneous, uniaxially birefringent medium, by means of the standard one-dimensional homogenization technique. This approach allows to expand the argumentation for the mode matching with anisotropic waveguides to the case of dielectric multilayers, with an important consequence that the mode matching is in principle possible with those structures too. To find the minimum number of layers required for the matching and to optimize the refractive index profile, we furthermore analyse the waveguiding conditions for TE and TM modes in multilayer structures, tracking the fruitful analogy with confined one-dimensional electron states problem quite profoundly investigated in the framework of classical quantum mechanics and solid-state physics.

2.1. Effective medium treatment

In a single-layer isotropic waveguide, the two given modes—TE (s-polarized) and TM (p-polarized)—are commonly characterized at a fixed frequency by definitely different propagation angles $\theta_{s,p}$ between the wavevector and the plane of the guide, and consequently, by different (non-equal) propagation constants $\beta_{s,p}$ via

$$\beta_{s,p} = n \cos \theta_{s,p}, \quad (1)$$

where n is the refractive index of the waveguiding medium and the subscripts s and p differentiate between TE and TM modes. Anisotropy of the waveguide accounts evidently for the following modification of equation (1):

$$\beta_{s,p} = n_{s,p}(\theta) \cos \theta_{s,p}, \quad (2)$$

where $n_{s,p}$ are the indices ‘seen’ by TE and TM modes, and a situation like that in figure 1 becomes possible, when the projections of the wave vectors of different modes onto the plane of guidance coincide, giving rise to the phenomenon of mode matching.

Consider now a two-component periodic multilayer system consisting of layers of dielectric permittivity $\epsilon_1 = n_1^2$ and thickness t_1 separated by layers with permittivity $\epsilon_2 = n_2^2$ and thickness t_2 . If a plane wave is incident onto this array with its electric vector \mathbf{E} polarized parallel to the layers (TE-wave) and the thicknesses t_1 and t_2 are small compared to the wavelength, then one may introduce the effective dielectric permittivity of the array as [12]

$$\epsilon_s = \frac{t_1 \epsilon_1 + t_2 \epsilon_2}{t_1 + t_2}, \quad (3)$$

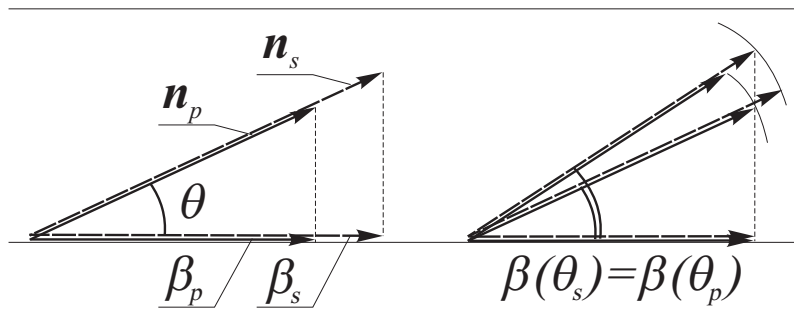


Figure 1. Refraction vectors $\mathbf{n}_{s,p} = n_{s,p}\tilde{\mathbf{k}}$ ($\tilde{\mathbf{k}}$ is the wave normal) and propagation constants $\beta_{s,p}$ in a birefringent waveguiding medium.

and if the magnetic vector \mathbf{H} is parallel to the plates (TM-wave), then the effective permittivity becomes [12]

$$\epsilon_p = \frac{(t_1 + t_2) \epsilon_1 \epsilon_2}{t_1 \epsilon_1 + t_2 \epsilon_2}. \quad (4)$$

This treatment allows one to state that two isonormal, s- and p-polarized waves ‘see’ in general different refractive indices of effective waveguiding medium, hence if to start from the isotropic ($n_1 = n_2$) case and then change one of the indices, the families of TE and TM dispersion curves will undergo non-equal shifts on the dispersion structure diagram and thus intersect at a number of points, displaying the modes degeneration—the perfect phase matching. One should remember by the way that it is of course not complete, spatial degeneration of modes, but mere propagation constant coincidence.

The question that naturally arises here is: How much layers are enough for the mode matching to occur? In other words: When does the reasoning based on the form birefringence approach lose its validity? To answer these questions and to elucidate the physics of mode matching in the case of a finite number of layers, one may find it convenient to employ an explicit mathematical analogy between confined photon and electron states, the latter being quite thoroughly investigated in classical quantum mechanics and solid-state physics—a comprehensible 1D Kronig–Penney model should certainly be mentioned here as an example.

2.2. Dispersion equation for TE and TM modes as an eigenproblem: Qualitative analysis

As is commonly known and excellently described by Joannopoulos *et al* [10, ch 3], symmetry considerations allow us to separate the modes of planar dielectric waveguides into two classes: TE and TM polarized. In a coordinate system in which the x -axis is normal to the bimedia interfaces and the light propagates along the z -direction, we can write for TE and TM polarizations, respectively,

$$\mathbf{E}(\mathbf{r}) = \exp(i\frac{\omega}{c}\beta z)\phi^E(x)\mathbf{y} \quad (5)$$

and

$$\mathbf{H}(\mathbf{r}) = \exp(i\frac{\omega}{c}\beta z)\phi^H(x)\mathbf{y}, \quad (6)$$

where ω is the angular frequency, c is the vacuum speed of light, β is what we call the propagation constant, $\phi^E(x)$ and $\phi^H(x)$ are the unknown field distributions. Substituting one of these fields into corresponding Maxwell wave equation, in the case of permittivity $\epsilon(\mathbf{r}) = \epsilon(x)$ being a step-wise function equal to n_j^2 for the j th homogeneous layer we obtain the following eigenproblem:

$$\frac{d^2\phi(x)}{dx^2} + \frac{\omega^2}{c^2}(n_j^2 - \beta^2)\phi(x) = 0. \quad (7)$$

This is the dispersion equation for a multilayer waveguide; the difference between TE and TM polarizations lies exclusively in different boundary conditions at the interfaces of the layers. Thus, at the interface $x = x_0$ we have:

$$\phi^E(x_0^-) = \phi^E(x_0^+), \quad \frac{d\phi^E(x_0^-)}{dx} = \frac{d\phi^E(x_0^+)}{dx}, \quad (8)$$

$$\phi^H(x_0^-) = \phi^H(x_0^+), \quad \frac{1}{\epsilon(x_0^-)} \frac{d\phi^H(x_0^-)}{dx} = \frac{1}{\epsilon(x_0^+)} \frac{d\phi^H(x_0^+)}{dx}. \quad (9)$$

Conditions for the derivatives originate from continuity of z -components of magnetic and electric field vectors via Maxwell equations for $\nabla \times \mathbf{E}$ and $\nabla \times \mathbf{H}$ respectively.

Note that the scalar Helmholtz wave equation (7) with boundary conditions for the TE mode (8) is isomorphous to the familiar stationary one-dimensional Schrödinger equation

$$\frac{d^2\psi(x)}{dx^2} + \frac{2m}{\hbar^2}(\mathcal{E} - U(x))\psi(x) = 0 \quad (10)$$

for a particle of mass m in potential energy profile $U(x)$, \mathcal{E} being the energy levels corresponding to eigenfunctions $\psi_{\mathcal{E}}(x)$.

The difference in boundary conditions for the derivatives of $\phi^E(x)$ and $\phi^H(x)$ functions leads to strict alternation of TE and TM dispersion curves of one- and two-layer waveguides. In other words, at a fixed frequency ω the propagation constants of confined TE modes are always separated by those of TM ones. This ‘rule’ can be illustrated by figure 2 for the lowest modes in a single-layer waveguide: the ratio $\lambda/2d$ (λ is the wavelength *within* the guide) for the $\phi^E(x)$ function of the TE₀ mode is obviously more than that for the TM₀ mode because of the steeper slopes of the $\phi^H(x)$ function near the interfaces due to the boundary conditions, but however high the refractive index of the guide and consequently the slopes of $\phi^H(x)$ function in vicinity of the interfaces may be, the ratio $\lambda/2d$ for the TM₀ mode will never drop below unity, while for the next TE mode—TE₁—it is definitely less than 1, actually lying between 1/2 and 1.

Similar argumentation still holds for the modal dispersion structure of a two-layer stack, no matter of the refractive index contrast of the layers, and, in general, for N -layer stack with refractive indices of the layers regularly increasing or decreasing throughout the array ($n_1 < n_2 < \dots < n_N$ or $n_1 > n_2 > \dots > n_N$).

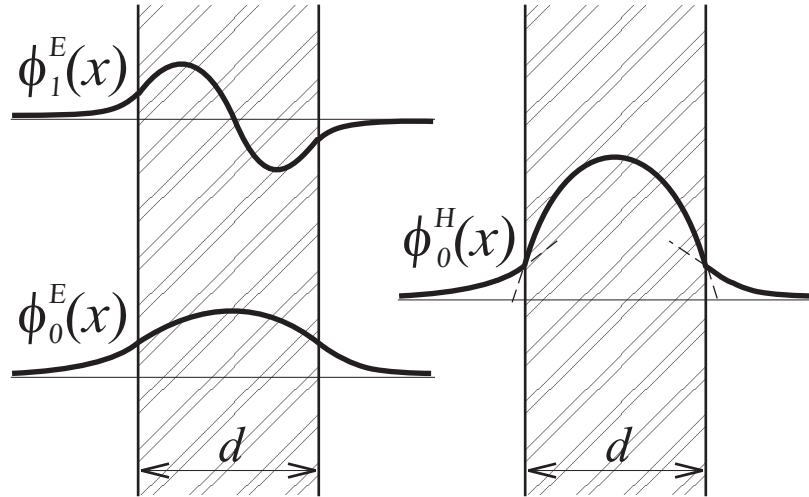


Figure 2. Illustration to the rule of alternation of TE and TM modes in a single-layer waveguide.

Surprisingly, a three-layer waveguide of step-wise refractive index profile develops considerably different from the above case, provided the second layer is of lower refractive index than its surroundings: $n_2 < n_{1,3}$. Also assume for the sake of simplicity $n_1 = n_3$ and, as before, symmetric sandwiching: $n_0 = 1$ for both ambient media. As it will now be argued, the mode matching can be effectively implemented with such a system; to understand its origin, it might be a helpful trick to recall the changes in the system of eigenfunctions $\psi_{\mathcal{E}}(x)$ of an electron in one-dimensional three-step potential gap, each step being of width $d/3$:

$$U(x) = \begin{cases} U_0 & \text{for } |x| > d/2 \text{ (outside the gap)} \\ U_2 & \text{for } |x| < d/6 \text{ (in the middle region)} \\ U_{1,3} & \text{otherwise (in the lateral regions)} \end{cases} \quad (11)$$

with increasing U_2 from $U_2 = U_{1,3}$ to $U_2 = U_0$ that corresponds to decreasing n_2 from $n_2 = n_{1,3}$ (isotropic single-layer waveguide) to unity (two waveguide channels separated by air region), the frequency ω being fixed.

While the difference between $U_{1,3}$ and U_2 is negligible, the energy levels correspondent to $\psi_{\mathcal{E}}(x)$ eigenfunctions compose a relatively regular discrete energy spectrum, and so do the propagation constants of TE modes at any fixed frequency. The TM mode spectrum is a bit shifted with respect to the TE one due to the difference in boundary conditions for the modes of different types, and as just emphasized, the propagation constants of TE and TM modes are strictly alternating.

By contrast, when U_2 is large enough, the regions of low potential become weakly coupled, the entire system possessing the twofold (generally N -fold, where N is the number of regions of low potential—or high refractive index) splitting of mixed odd and even energy levels corresponding to nearly degenerate TE modal *groups* of N modes each. TM modes also form similar N -fold groups which are, however, shifted

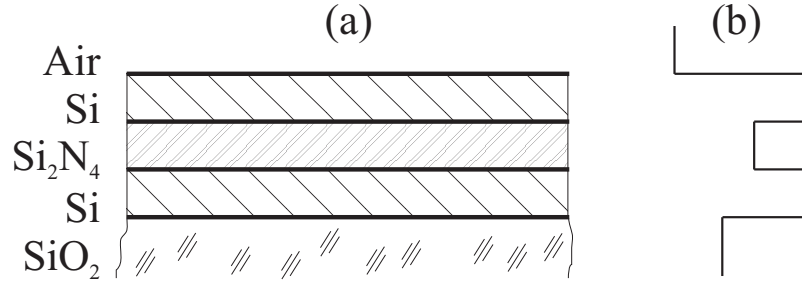


Figure 3. (a) Schematic diagram of the three-layer dielectric waveguide on silica substrate and (b) its refractive index profile.

with respect to TE groups. It is clear now that for certain n_2 lying between those extremes, or equivalently, for certain frequency ω in case of n_2 being somewhat less than $n_{1,3}$ and fixed, the matching of TE and TM modes should be expected, with the only exception for TE_0 mode in agreement with the inevitably negative character of form birefringence [12, 13]. We can also anticipate herefore that the minimum sufficient number of layers for the perfect phase matching is three, provided the central layer is of lower refractive index than the surrounding ones—see figure 3 for an example of such a structure. More generally, the refractive index profile of the waveguide should have more than one maximum for the effective mode matching.

Consider now a kind of three-layer system ‘reciprocal’ to the above—with a middle layer being of higher index than the lateral ones. For this third possible arrangement of the layers, the mode matching is not forbidden, yet there is seemingly no solid ground to expect the matching of the lowest modes now since such a system appears to stand close to conventional slab waveguide—the latter with no possibility for the mode matching at all. More thorough analysis in the manner above for a single-layer waveguide shows that coincidence of propagation constants should be expected for the modes *of the same order*, but as before with the exception of TE_0 and TM_0 modes. It is demonstrated in section 4 that the mode matching is indeed observed in this case only in the multimode regime, thus actually losing its practical value.

3. Dispersion analysis for multiperiod two- and three-layer waveguides

The general form (7)–(9) of the dispersion equations for guided modes is quite good for qualitative analysis, but inconvenient for numerical investigations into the TE and TM mode spectra of multilayer stacks. In the current section we render the known dispersion relations for multiperiod bilayer waveguides and present their generalization for three-layer multiperiod systems. Thus, following Yeh [14], in case of an N -period stack with a *bilayer* unit cell one has for TE modes:

$$\frac{\sin(N\Lambda_{2s})}{\sin \Lambda_{2s}} \left[\left(\frac{1}{\xi_{Sub}} + \frac{1}{\xi_{Cov}} \right) CC - \left(\frac{\eta_1}{\xi_{Sub}} + \frac{\eta_2}{\xi_{Cov}} \right) SS \right]$$

$$\begin{aligned}
& - \left(\frac{\eta_1}{\xi_{Sub}\xi_{Cov}} - \frac{1}{\eta_2} \right) \text{SC} - \left(\frac{\eta_2}{\xi_{Sub}\xi_{Cov}} - \frac{1}{\eta_1} \right) \text{CS} \Big] \\
& - \left(\frac{1}{\xi_{Sub}} + \frac{1}{\xi_{Cov}} \right) \frac{\sin[(N-1)\Lambda_{2s}]}{\sin \Lambda_{2s}} = 0,
\end{aligned} \tag{12}$$

where

$$\Lambda_{2s} = \arccos \left[\text{CC} - \left(\frac{\eta_1}{\eta_2} + \frac{\eta_2}{\eta_1} \right) \frac{\text{SS}}{2} \right], \tag{13}$$

$\eta_j = \sqrt{n_j^2 - \beta^2}$, $\xi_{Sub,Cov} = \sqrt{\beta^2 - n_{Sub,Cov}^2}$ and the shorthand notation such as SC stands for the corresponding harmonic function product, in the case above, $\sin(kt_1n_1) \cos(kt_2n_2)$, with the free-space wave number $k = \omega/c$.

Likewise for TM modes [14]:

$$\begin{aligned}
& \frac{\sin(N\Lambda_{2p})}{\sin \Lambda_{2p}} \left[\left(\frac{\xi_{Sub}}{\epsilon_{Sub}} + \frac{\xi_{Cov}}{\epsilon_{Cov}} \right) \text{CC} - \left(\frac{\xi_{Sub}\epsilon_1\eta_2}{\epsilon_{Sub}\epsilon_2\eta_1} + \frac{\xi_{Cov}\epsilon_2\eta_1}{\epsilon_{Cov}\epsilon_1\eta_2} \right) \text{SS} \right. \\
& \left. - \left(\frac{\eta_1}{\epsilon_1} + \frac{\xi_{Sub}\xi_{Cov}\epsilon_1}{\epsilon_{Sub}\epsilon_{Cov}\eta_1} \right) \text{SC} - \left(\frac{\eta_2}{\epsilon_2} + \frac{\xi_{Sub}\xi_{Cov}\epsilon_2}{\epsilon_{Sub}\epsilon_{Cov}\eta_2} \right) \text{CS} \right] \\
& - \left(\frac{\xi_{Sub}}{\epsilon_{Sub}} + \frac{\xi_{Cov}}{\epsilon_{Cov}} \right) \frac{\sin[(N-1)\Lambda_{2p}]}{\sin \Lambda_{2p}} = 0,
\end{aligned} \tag{14}$$

where

$$\Lambda_{2p} = \arccos \left[\text{CC} - \left(\frac{\eta_1\epsilon_2}{\eta_2\epsilon_1} + \frac{\eta_2\epsilon_1}{\eta_1\epsilon_2} \right) \frac{\text{SS}}{2} \right]. \tag{15}$$

The above equations look rather awkward, but they can be easily handled and promptly solved numerically in any mathematical computing package.

Three-layer semi-infinite dielectric superlattices have been studied earlier, but with the focus on the existence and the dispersion of bulk and surface polaritons [15]. In the case of a *finite*, N -period stack with a trilayer unit cell one can however quite trivially derive the following dispersion relation for the guided TE modes (see the appendix for the details):

$$\begin{aligned}
& \frac{\sin(N\Lambda_{3s})}{\sin \Lambda_{3s}} \left[\left(\frac{1}{\xi_{Sub}} + \frac{1}{\xi_{Cov}} \right) \text{CCC} - \left(\frac{\eta_2}{\eta_1\eta_3} + \frac{1}{\xi_{Sub}\xi_{Cov}} \frac{\eta_1\eta_3}{\eta_2} \right) \text{SSS} \right. \\
& - \left(\frac{1}{\xi_{Sub}} \frac{\eta_1}{\eta_2} + \frac{1}{\xi_{Cov}} \frac{\eta_2}{\eta_1} \right) \text{SSC} - \left(\frac{1}{\xi_{Sub}} \frac{\eta_1}{\eta_3} + \frac{1}{\xi_{Cov}} \frac{\eta_3}{\eta_1} \right) \text{SCS} \\
& - \left(\frac{1}{\xi_{Sub}} \frac{\eta_2}{\eta_3} + \frac{1}{\xi_{Cov}} \frac{\eta_3}{\eta_2} \right) \text{CSS} - \left(\frac{\eta_1}{\xi_{Sub}\xi_{Cov}} + \frac{1}{\eta_1} \right) \text{SCC} \\
& - \left(\frac{\eta_2}{\xi_{Sub}\xi_{Cov}} + \frac{1}{\eta_2} \right) \text{CSC} - \left(\frac{\eta_3}{\xi_{Sub}\xi_{Cov}} + \frac{1}{\eta_3} \right) \text{CCS} \Big] \\
& - \left(\frac{1}{\xi_{Sub}} + \frac{1}{\xi_{Cov}} \right) \frac{\sin[(N-1)\Lambda_{3s}]}{\sin \Lambda_{3s}} = 0,
\end{aligned} \tag{16}$$

where

$$\Lambda_{3s} = \arccos \left[\text{CCC} - \left(\frac{\eta_1}{\eta_2} + \frac{\eta_2}{\eta_1} \right) \frac{\text{SSC}}{2} - \frac{1}{2} \left(\frac{\eta_1}{\eta_3} + \frac{\eta_3}{\eta_1} \right) \frac{\text{SCS}}{2} - \frac{1}{2} \left(\frac{\eta_2}{\eta_3} + \frac{\eta_3}{\eta_2} \right) \frac{\text{CSS}}{2} \right], \quad (17)$$

and for TM modes:

$$\begin{aligned} & \frac{\sin(N\Lambda_{3p})}{\sin \Lambda_{3p}} \left[\left(\frac{\xi_{Sub}}{\epsilon_{Sub}} + \frac{\xi_{Cov}}{\epsilon_{Cov}} \right) \text{CCC} - \left(\frac{\xi_{Sub}\xi_{Cov}\epsilon_1\eta_3}{\epsilon_{Sub}\epsilon_{Cov}\epsilon_2\eta_1\eta_3} + \frac{\epsilon_2}{\epsilon_1\eta_3} \frac{\eta_1\eta_3}{\eta_2} \right) \text{SSS} \right. \\ & - \left(\frac{\xi_{Sub}\epsilon_1\eta_2}{\epsilon_{Sub}\epsilon_2\eta_1} + \frac{\xi_{Cov}\epsilon_2\eta_1}{\epsilon_{Cov}\epsilon_1\eta_2} \right) \text{SSC} - \left(\frac{\xi_{Sub}\epsilon_1\eta_3}{\epsilon_{Sub}\epsilon_3\eta_1} + \frac{\xi_{Cov}\epsilon_3\eta_1}{\epsilon_{Cov}\epsilon_1\eta_3} \right) \text{SCS} \\ & - \left(\frac{\xi_{Sub}\epsilon_2\eta_3}{\epsilon_{Sub}\epsilon_3\eta_2} + \frac{\xi_{Cov}\epsilon_3\eta_2}{\epsilon_{Cov}\epsilon_2\eta_3} \right) \text{CSS} - \left(\frac{\eta_1}{\epsilon_1} + \frac{\xi_{Sub}\xi_{Cov}\epsilon_1}{\epsilon_{Sub}\epsilon_{Cov}\eta_1} \right) \text{SCC} \\ & - \left. \left(\frac{\eta_2}{\epsilon_2} + \frac{\xi_{Sub}\xi_{Cov}\epsilon_2}{\epsilon_{Sub}\epsilon_{Cov}\eta_2} \right) \text{CSC} - \left(\frac{\eta_3}{\epsilon_3} + \frac{\xi_{Sub}\xi_{Cov}\epsilon_3}{\epsilon_{Sub}\epsilon_{Cov}\eta_3} \right) \text{CCS} \right] \\ & - \left(\frac{\xi_{Sub}}{\epsilon_{Sub}} + \frac{\xi_{Cov}}{\epsilon_{Cov}} \right) \frac{\sin[(N-1)\Lambda_{3p}]}{\sin \Lambda_{3p}} = 0, \quad (18) \end{aligned}$$

where

$$\Lambda_{3p} = \arccos \left[\text{CCC} - \left(\frac{\eta_1\epsilon_2}{\eta_2\epsilon_1} + \frac{\eta_2\epsilon_1}{\eta_1\epsilon_2} \right) \frac{\text{SSC}}{2} - \left(\frac{\eta_1\epsilon_3}{\eta_3\epsilon_1} + \frac{\eta_3\epsilon_1}{\eta_1\epsilon_3} \right) \frac{\text{SCS}}{2} - \left(\frac{\eta_2\epsilon_3}{\eta_3\epsilon_2} + \frac{\eta_3\epsilon_2}{\eta_2\epsilon_3} \right) \frac{\text{CSS}}{2} \right]. \quad (19)$$

Of course, certain symmetries could obviously be found in these equations, but still the latter seem to be too cumbersome for any qualitative speculations. Instead, one can easily do now plenty of computational work related to physically realizable multilayers, and in the following section we will do that with waveguides made of such popular optical materials as silicon and its compounds.

4. Simulated results for multilayers of silicon and silicon nitride

To demonstrate the performance of dielectric multilayers for the mode matching and to corroborate theoretical considerations presented in section 2, we have plotted in figure 4 the modal dispersion curves of (a) two-layer Si/Si₃N₄ and (b) three-layer Si/Si₃N₄/Si waveguides, as well as of (c,d) their two-period counterparts. Silicon and its nitride have been chosen deliberately since these materials are found to be suitable for manifold passive optical components like branching waveguides, couples, interconnects, interferometers, power splitters, and filters [16, 17]. We employed here the mode dispersion relations for bilayer and three-layer waveguides and their generalization for multiperiod systems, equations (12)–(19). The thicknesses of the layers were assumed to be equal; the refractive indices are 3.5 (Si), 2.0 (Si₃N₄) and 1.5 (SiO₂). All the numerical calculations were performed with Mathematica 4.1 [18].

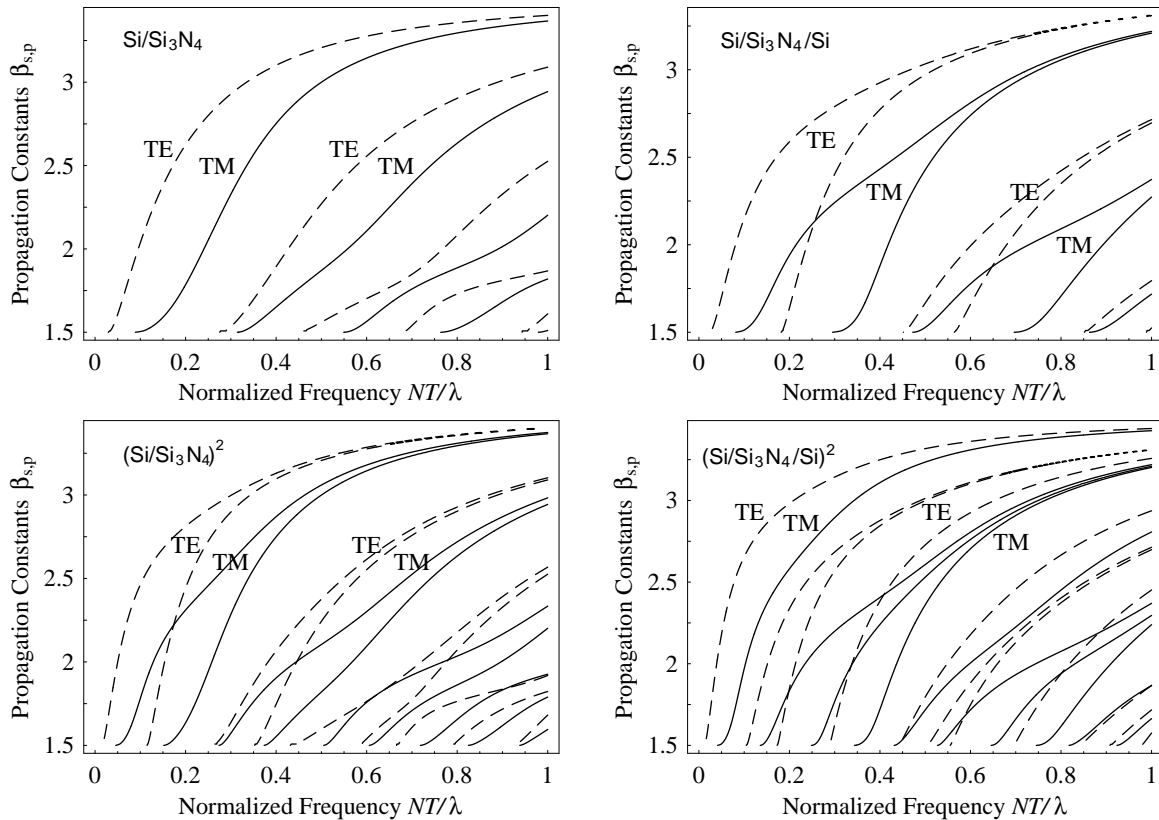


Figure 4. TE (---) and TM (—) families of the modal dispersion curves for (a) bilayer Si/Si₃N₄, (b) three-layer Si/Si₃N₄/Si, (c) two-period four-layer (Si/Si₃N₄)² and (d) five-layer (Si/Si₃N₄/Si)² waveguides, all on silica substrate.

Figure 4(a) is of no particular interest—we see the system of TE and TM dispersion curves that is quite typical for slab dielectric waveguides, with just slight perturbations of the high-order modal curves near $\beta \approx 2$ —that is close to the refractive index of the middle layer. In contrast, figure 4(b) reveals the predicted intersection of modal dispersion curves for the three-layer system; for the first phase-matching point where the TM₀ mode matches TE₁ at $NT = 0.25\lambda$ (here T is the total thickness of one period, so that NT gives the thickness of the whole structure), we can estimate the thicknesses of the layers to be $t_1 = t_2 = t_3 = 130$ nm for operation near 1.55 μm , i.e. in the spectral range for telecommunication frequencies. In order to improve the operation bandwidth, the slopes of dispersion curves at the given point of intersection must be as close as possible, and for that purpose the refractive index distribution should be further optimized.

The comparison between figures 4(b), (c) and (d) confirms that it is the number of layers of high refractive index, and not periods—which sometimes are more ‘mental’ constructs than ‘physical’ objects—that determines the number of modes in the TE and TM bands formed. Thus, for both Si/Si₃N₄/Si and (Si/Si₃N₄)² structures constituted of two silicon layers—two ‘potential gaps’ for photons—the twofold grouping of modes at high β values is clearly observed. Finally, figure 5 testifies to the statement of section 2

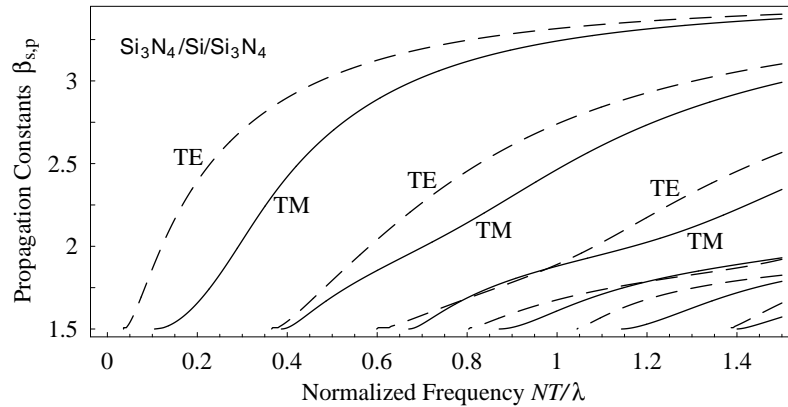


Figure 5. Modal dispersion curves for three-layer $\text{Si}_3\text{N}_4/\text{Si}/\text{Si}_3\text{N}_4$ waveguide on silica substrate—the ‘reverse’ structure of that in figure 4(b).

that for the effective mode matching, the refractive index of the medium layer in three-layer waveguide should be low enough; otherwise, the matching is not forbidden, but occurs only for high-order modes and remains thus impracticable.

5. Conclusion

In summary, the perfect phase matching of TE and TM guided modes with a multilayer waveguide composed of linear isotropic dielectric materials has been anticipated and simulated for the first time. Dielectric superlattices with unit cells of two types have been considered: two-layer and tree-layer; for finite, N -period, three-component structures, the compact analytical expressions for the mode dispersion have been derived, which can be regarded as a self-sufficient result.

Numerical simulations performed for a silicon—silicon-nitride—silicon waveguide on a silica substrate bear witness that even a three-layer stack can be designed to exhibit at certain frequencies the perfect phase matching of TE and TM guided modes. Since the TE and TM mode spectra are naturally very sensitive to refractive index distribution, i.e. to the index contrast of the layers and their thicknesses, number and succession, wide possibilities arise to tailor the mode dispersion in the vicinity of those phase-matching points.

The principle of perfect phase matching with a multilayer dielectric array has important potential implementations in polarization-insensitive planar propagation, fibre-to-planar waveguide coupling, mode conversion, filtering etc. The advantage of the presented device scheme is its simplicity and compatibility with common integrated optics techniques, e.g. with planar optical waveguide technology. Further important issues to be addressed for the development of applicational aspects of the scheme are optimization with a more advanced refractive index profile of the waveguiding stack and integration into complex, state-of-the-art optical and optoelectronic elements.

Appendix

To derive the mode dispersion relation for the finite, N -period, three-layer dielectric superlattices, one can simply follow Yeh's [14] reasoning for bilayer multiperiod waveguides, yet we prefer to utilize another tool here—the general, dyadic-based formalism for stratified media [19] which proves to be a competitive modification of Berreman 4×4 matrix approach [20] and can be directly applied to more complicated problems of light scattering and confined propagation in, e.g., magnetized, metallo-dielectric and anisotropic arrays.

Consider an N -period three-layer stack sandwiched between isotropic, homogeneous, semi-infinite media—a substrate of permittivity ϵ_{Sub} and a cover of permittivity ϵ_{Cov} . The covariant dispersion relation for plane-stratified media [19] takes the form

$$\det \left[(-\gamma_{Sub}, \mathcal{I}) \times (\mathcal{P}_1 \mathcal{P}_2 \mathcal{P}_3)^N \times \begin{pmatrix} \mathcal{I} \\ -\gamma_{Cov} \end{pmatrix} \right] = 0, \quad (\text{A.1})$$

where $\mathcal{I} = \mathbf{z} \otimes \mathbf{z} + \mathbf{y} \otimes \mathbf{y}$ is the unit 2-D dyadic, \mathbf{z} and \mathbf{y} are the unit vectors in the plane of the guide, respectively parallel and perpendicular to the direction of propagation, $\mathbf{a} \otimes \mathbf{b}$ denotes the outer product $a_\alpha b_\beta$, \mathcal{P}_j is the evolution operator (4×4 matrix) that relates z and y components of electric and magnetic fields arranged into truncated $\mathbf{x} \times \mathbf{E} = (-E_z, E_y)^T$ and $\mathbf{H}_\tau = (H_y, H_z)^T$ vectors at the interfaces $x = x_j$ and $x = x_{j-1}$ of the j th layer,

$$\begin{pmatrix} \mathbf{H}_\tau(x_j) \\ \mathbf{x} \times \mathbf{E}(x_j) \end{pmatrix} = \mathcal{P}_j \begin{pmatrix} \mathbf{H}_\tau(x_{j-1}) \\ \mathbf{x} \times \mathbf{E}(x_{j-1}) \end{pmatrix}, \quad (\text{A.2})$$

and $\gamma_{Sub}, \gamma_{Cov}$ are the impedance tensors of the ambient media that allow to generate \mathbf{H}_τ given $\mathbf{x} \times \mathbf{E}$: $\mathbf{H}_\tau = \gamma(\mathbf{x} \times \mathbf{E})$,

$$\gamma_{Sub,Cov} = \frac{1}{i\xi_{Sub,Cov}} \mathbf{z} \otimes \mathbf{z} + \frac{i\xi_{Sub,Cov}}{\epsilon_{Sub,Cov}} \mathbf{y} \otimes \mathbf{y}. \quad (\text{A.3})$$

In the case of an isotropic dielectric layer, the evolution matrix is

$$\begin{aligned} \mathcal{P}_j &= {}^z\mathcal{P}_j \mathbf{z} \otimes \mathbf{z} + {}^y\mathcal{P}_j \mathbf{y} \otimes \mathbf{y} \\ &= \begin{pmatrix} C_j & i\eta_j S_j \\ (i/\eta_j)S_j & C_j \end{pmatrix} \mathbf{z} \otimes \mathbf{z} + \begin{pmatrix} C_j & (i\epsilon_j/\eta_j)S_j \\ (i\eta_j/\epsilon_j)S_j & C_j \end{pmatrix} \mathbf{y} \otimes \mathbf{y}. \end{aligned} \quad (\text{A.4})$$

Such a simple structure of operators \mathcal{P}_j and $\gamma_{Sub,Cov}$ permits us to decompose dispersion equation (A1) into two separate equations—for TE and TM modes; these are obtained via multiplying ${}^z\mathcal{P}_1, {}^z\mathcal{P}_2, {}^z\mathcal{P}_3$ or ${}^x\mathcal{P}_1, {}^x\mathcal{P}_2, {}^x\mathcal{P}_3$ and applying the known representation of N th power of a 2×2 unimodular matrix in terms of the Chebychev polynomials of the second kind given by Abelès [21]. Finally, this cumbersome, but physically transparent procedure results in equations (16)–(19).

References

- [1] Tien P K, Schinke D P and Blank S L 1974 Magneto-optics and motion of the magnetization in a film-waveguide optical switch *J. Appl. Phys.* **45** 3059–68

- [2] Bruns W K and Milton A F 1975 Mode conversion in planar-dielectric separating waveguides *IEEE J. Quantum Electron.* **11** 32–9
- [3] Gillies J R and Hlawiczka P 1976 TE and TM modes in gyrotropic waveguides *J. Phys. D: Appl. Phys.* **9** 1315–22
- [4] Hlawiczka P 1978 A gyrotropic waveguide with dielectric boundaries: the longitudinally magnetised case *J. Phys. D: Appl. Phys.* **11** 1157–66
- [5] Hlawiczka P 1978 The gyrotropic waveguide with a normal applied DC field *J. Phys. D: Appl. Phys.* **11** 1941–8
- [6] Winn J N, Fink Y, Fan S, Joannopoulos J D 1998 Omnidirectional reflection from a one-dimensional photonic crystal *Opt. Lett.* **23** 1573–5
- [7] Dowling J P 1998 Mirror on the wall: you're omnidirectional after all? *Science* **288** 1841–2
- [8] Chigrin D N, Lavrinenko A V, Yarotsky D A and Gaponenko S V 1999 Observation of total omnidirectional reflection from a one-dimensional dielectric lattice *Appl. Phys. A* **68** 25–8
- [9] Russell P St J, Tredwell S and Roberts R J 1999 Full photonic band-gaps and spontaneous emission control in 1-D multilayer dielectric structures *Opt. Commun.* **160** 66–71
- [10] Joannopoulos J D, Meade R D and Winn J N 1995 *Photonic Crystals: Molding the Flow of Light* (Princeton, NJ: Princeton University Press)
- [11] Lavrinenko A V, Shyroki D N and Zhilko V V 2002 Guided and leaky modes in magneto-optical sandwiches with ultrathin metal films *J. Magn. Magn. Mater.* **247** 171–7
- [12] Born M and Wolf E 1968 4th edn *Principles of Optics* (Oxford: Pergamon) ch 14
- [13] Gu C and Yeh P 1996 Form birefringence dispersion in periodic layered media *Opt. Lett.* **21** 504–6
- [14] Yeh P 1988 *Optical Waves in Layered Media* (New York: Wiley) ch 11
- [15] Mendialdua J, Rodriguez A, More M, Akjouj A and Dobrzynski L 1994 Bulk and surface phonon polaritons in three-layer superlattices *Phys. Rev. B* **50** 14 605–8
- [16] Wörhoff K, Lambeck P V and Driessen A 1999 Design, tolerance analysis, and fabrication of silicon oxynitride based planar waveguides for communication devices *J. Lightwave Technol.* **17** 1401–7
- [17] Schauwecker B, Arnold M, Radehaus C V, Przyrembel G and Kuhlow B 2002 Optical waveguide components with high refractive index difference in silicon-oxynitride for application in integrated optoelectronics *Opt. Eng.* **41** 237–43
- [18] Wolfram research (www.wolfram.com)
- [19] Barkovskii L M, Borzdov G N and Lavrinenko A V 1987 Fresnel's reflection and transmission operators for stratified gyroanisotropic media *J. Phys. A: Math. Gen.* **20** 1095–106
- [20] Berreman D W 1972 Optics in stratified and anisotropic media: 4×4 -matrix formulation *J. Opt. Soc. Am* **62** 502–10
- [21] Abelès F 1950 Reserches sur la propagation des ondes electromagnetiques sinusoidales dans les milieux stratifiés. Application aux couches minces *Ann. Physique* **5** 596–640